J Radioanal Nucl Chem (2013) 295:523–536
DOI 10.1007/s10967-012-2015-4

Time resolution investigations for general purpose plastic scintillation detectors in different thicknesses

E. E. Ermis · C. Celiktas

Received: 10 April 2012 / Published online: 22 August 2012
© Akadémiai Kiadó, Budapest, Hungary 2012

Abstract Time spectra of ^{90}Sr, ^{137}Cs and ^{207}Bi radioactive sources were obtained by using a BC 400 type plastic scintillation detectors in different thicknesses. Time resolution values through the time spectra were obtained by means of leading edge and constant fraction timing methods. The obtained time resolution values from leading edge method were compared with those of constant fraction timing method.

Keywords ^{90}Sr · ^{137}Cs · ^{207}Bi · Plastic scintillation detector · Leading edge timing method · Constant fraction timing method

Introduction

Very small time intervals between the events (i.e., charged particles have crossed a detector) are determined by means of timing measurements [1]. Special techniques are required for accurate measurements of these time intervals [2]. These techniques are called as timing methods.

Several different radiation detectors are used in timing measurements. Some of these are plastic scintillation, NaI(Tl) scintillation, multiwire proportional and semiconductor detectors. However, the best time resolution values are obtained from the plastic scintillators for different applications such as n–γ discrimination and neutrons in time-of-flight experiments [3].

E. E. Ermis · C. Celiktas (✉)
Physics Department, Faculty of Science, Ege University, 35100 Bornova, Izmir, Turkey
e-mail: cceliktas@yahoo.com

The measurement of the distribution of the time delays between prompt events gives the time resolution of a timing system [3]. Full width at half maximum value of a time spectrum determines the time resolution of the system (Fig. 1). The uncertainty of the timing system is determined by FWHM of the time spectrum [4]. The time value that corresponds to 61 % of the peak amplitude is called as shaping time. The peaking time is roughly 3–5 times greater than the shaping time (Fig. 1) [5].

Walk and jitter are the most important sources of the time uncertainty. The variations of the amplitudes or rise times of the signals give rise to the walk effect (Fig. 2). Time jitter (Fig. 3) is generated by noise and statistical fluctuations in the original detector signal [2]. The range between the noise level and the maximum output voltage is defined as dynamic range in a time–voltage diagram (Fig. 4) [5].

One of the most commonly and widely used plastics is polyvinytoluene [2]. BC 400 type general purpose plastic scintillators have higher light output and more economical than the other plastic scintillators [7].

The time resolution values of the time spectra which were obtained by using coincidence measurement were calculated by Abuelhia et al. [8]. Puzovic et al. examined the amplitude walk effect via leading edge timing method [9]. n/γ separation was achieved through the pulse shape discrimination method by Zaitseva et al. [10].

Since the figure of merit of a timing system is the time resolution, we calculated time resolution values of the presented timing systems here which were consisted of plastic scintillation detectors in different thicknesses for ^{90}Sr, ^{137}Cs and ^{207}Bi by using leading edge and constant fraction timing methods. We also compared the obtained time resolution values from leading edge timing method with those of constant fraction timing method.

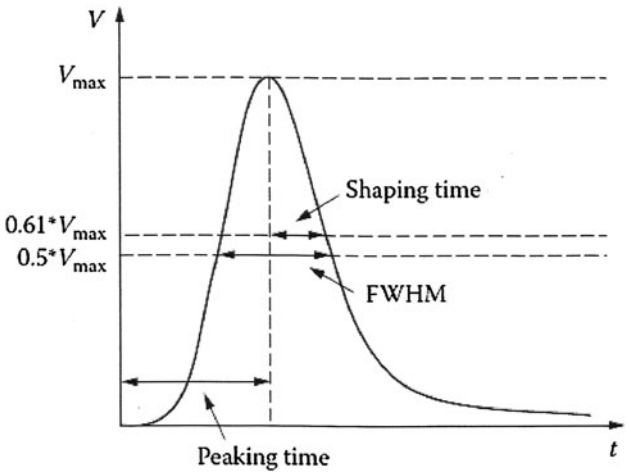


Fig. 1 Definitions of the shaping and peaking times [5]

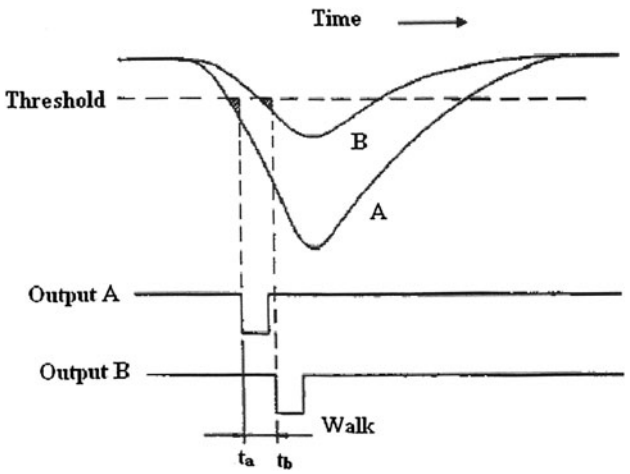


Fig. 2 Walk in a discriminator [2]

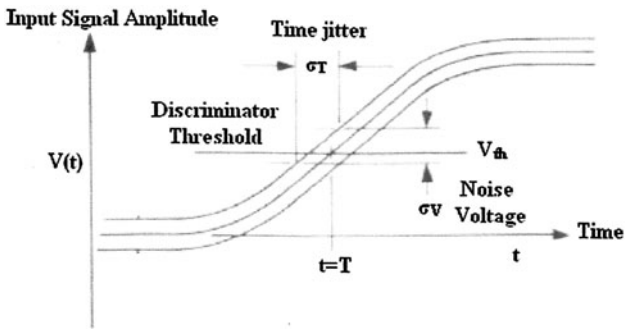


Fig. 3 Time jitter and noise voltage [6]

Experimental

In this study, ^{90}Sr, ^{137}Cs and ^{207}Bi standard radioactive sources were used. The half-lives and activities of the used sources are given Table 1. These sources were placed in 2 cm far away from the detector surface. Bicron BC 400 type plastic scintillation detectors which have 3 mm × 3 inch, 0.3 mm × 3 inch and 9 mm × 3 inch dimensions were used. Ambient light intensity and room temperature change cause to detector noise [2]. For this reason, all measurements were carried out in a dark medium and at a constant room temperature (22 °C) to prevent this electronic noise. Data acquisition time was chosen of 300 s in the study.

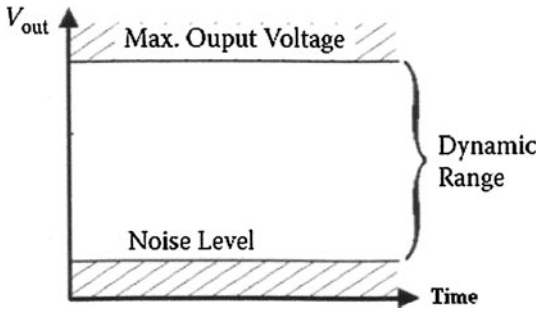


Fig. 4 Dynamic range [5]

Table 1 Half-lives and activities of the used radioactive sources [11]

Radioactive source	Half-life (year)	Activity (μCi)
^{90}Sr	28.78	0.100
^{137}Cs	30.07	5.000
^{207}Bi	31.55	9.468

The time of arrival of a pulse is determined by a discriminator in the leading edge timing method (Fig. 5). A discriminator threshold is set to a significant level (discriminator level). When the pulse crosses the discriminator level, the time of arrival of the pulse is determined [12].

Block diagram of the leading edge timing method is given in Fig. 6.

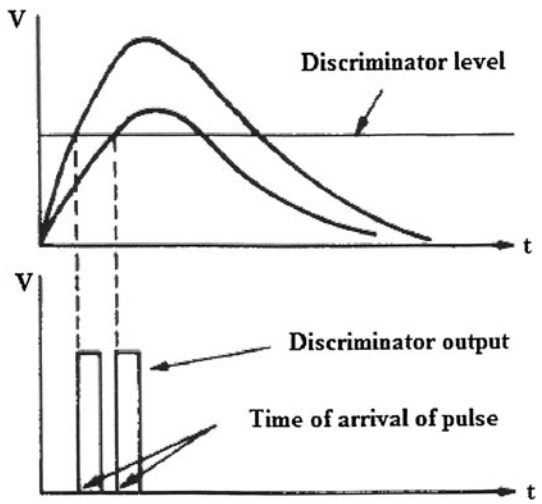


Fig. 5 The principle of the leading edge timing method [12]

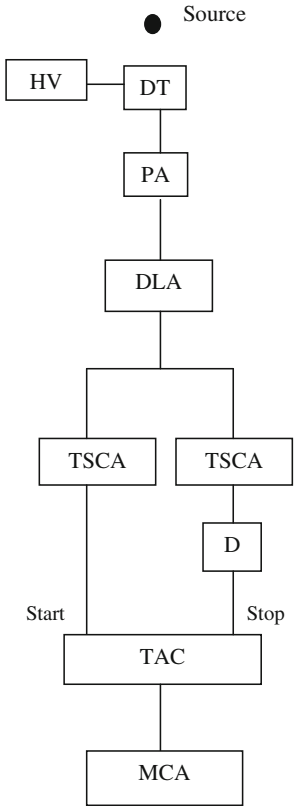


Fig. 6 *Block diagram* of the leading edge timing method circuit (*HV* high voltage supplier, *DT* detector, *PA* preamplifier, *DLA* delay line amplifier, *TSCA* timing single channel analyzer, *D* delay, *TAC* time to amplitude converter, *MCA* multichannel analyzer)

As shown in Fig. 6, the detector output was sent to a preamplifier (PA, Ortec 113). PA output was forwarded to a delay line amplifier (DLA, Ortec 460). The output of the DLA was split into two branches. Each branch was connected to a timing single channel analyzer (TSCA, Ortec 420A). One of the output signals of the TSCAs was directly sent to start input of a time to amplitude converter (TAC, Ortec 566), the other output was connected to stop input of the TAC through a delay unit (D, Ortec 425A). TAC is a device which converts a time period between its two input pulses into a logic output pulse whose height is proportional to this duration [2]. The output of the TAC was sent to input of a multichannel analyzer (MCA, Ortec Trump 8K). Consequently, the time spectra of the used radioactive sources were obtained.

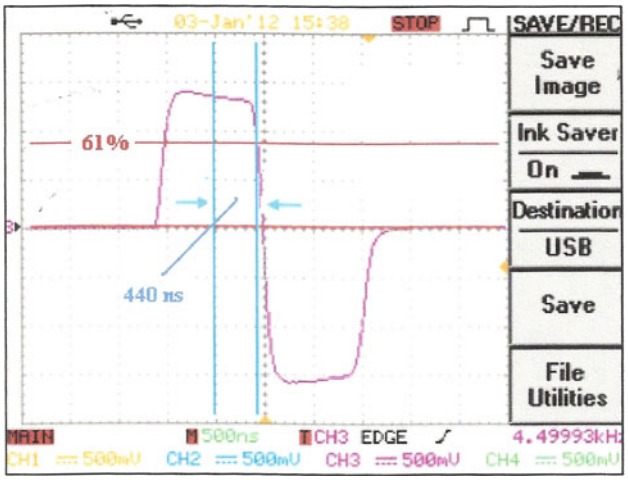


Fig. 8 The demonstration of peaking and shaping times on the DLA output signal

The output signal shapes of the PA and the TAC are shown in Fig. 7.

Integration time of the DLA was set to 0.04 μs according to the instructions in the manual of this device [13]. We found that the shaping time of the DLA was 440 ns through its output signal shape as indicated in Fig. 8.

Time jitter and noise voltage were determined from the TSCA output (Fig. 9).

Time jitter and noise voltage values with the dynamic range of 2:1 for the used detectors are given in Tables 2, 3 and 4.

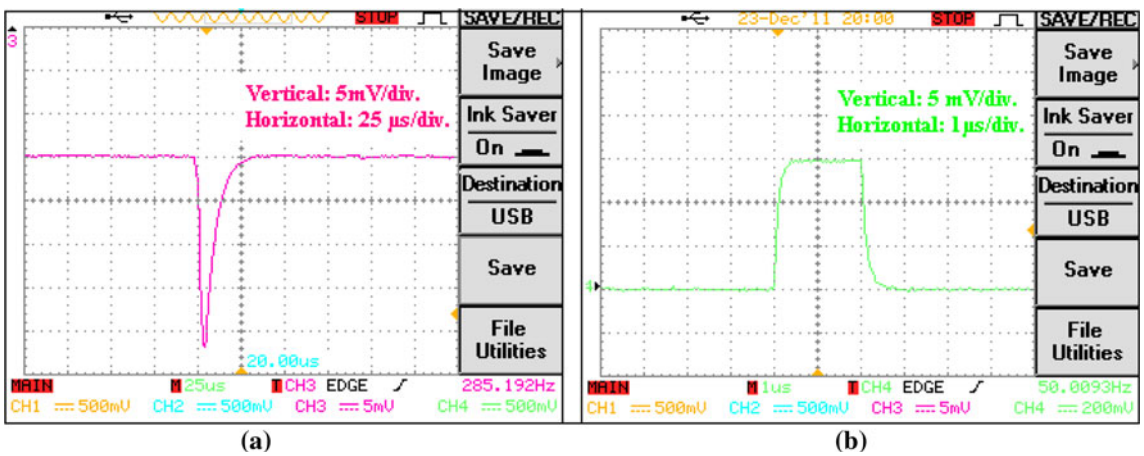


Fig. 7 Output signal shapes of **a** PA, **b** TAC

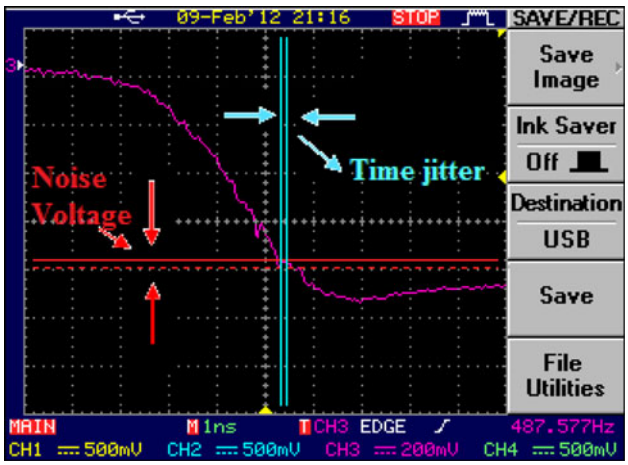


Fig. 9 Time jitter and noise voltage

Table 2 Time jitter and noise voltages for the used radioisotopes (3 mm × 3 inch detector) in leading edge timing method

Source	Time jitter (ps) (σ_T)	Noise voltage (mV) (σ_V)
^{90}Sr	120	≈24
^{137}Cs	120	≈24
^{207}Bi	120	≈24

Table 3 Time jitter and noise voltages for the used radioisotopes (0.3 mm × 3 inch detector) in leading edge timing method

Source	Time jitter (ps) (σ_T)	Noise voltage (mV) (σ_V)
^{90}Sr	120	≈32
^{137}Cs	120	≈32
^{207}Bi	120	≈32

Table 4 Time jitter and noise voltages for the used radioisotopes (9 mm × 3 inch detector) in leading edge timing method

Source	Time jitter (ps) (σ_T)	Noise voltage (mV) (σ_V)
^{90}Sr	120	≈32
^{137}Cs	120	≈32
^{207}Bi	120	≈24

In this work, the used second method was constant fraction timing method. The constant fraction timing is the most efficient and versatile method in order to produce walk-free timing signal since the logic signal is produced at a constant fraction of the peak height [2]. In Fig. 10, the principle of the constant fraction timing method is shown. The original pulse is attenuated by a factor f. The original

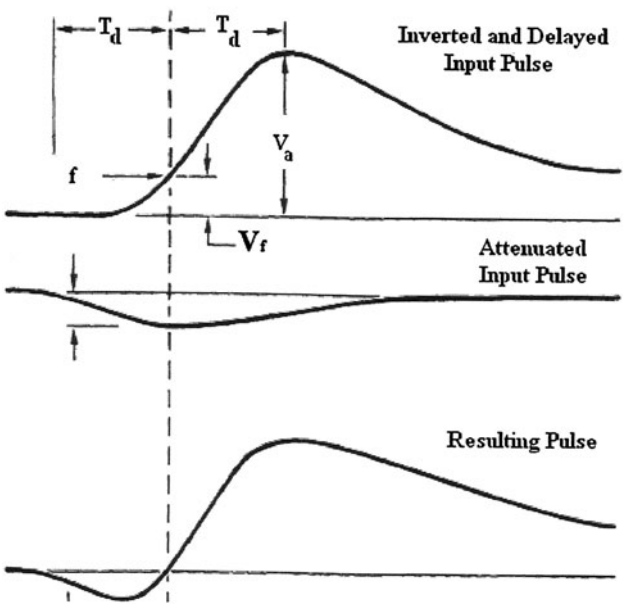


Fig. 10 Constant fraction timing method [14]

pulse is inverted and delayed for a time longer than its rise time. Finally, the pulses are added [12].

Constant fraction f is defined as the ratio of threshold voltage of constant fraction discriminator to the amplitude of the signal in constant fraction timing method [3, 15]. Furthermore, effective constant fraction value (f_{eff}) for the linear input signals is given as follows:

$$f_{eff} = \frac{f t_d}{t_r(1-f)} \quad (1)$$

where t_d and t_r are the internal delay time of the discriminator and the rise time of the signal, respectively. f_{eff} is always lower than f. t_d (delay time) in Eq. (1) is equal to $t_r(1-f)$ or lower than this value [16, 17]:

$$t_d \leq t_r(1-f) \quad (2)$$

In Fig. 11, the block diagram for the constant fraction timing method is shown.

In the constant fraction timing setup, the detector output was split into two branches, and these outputs were forwarded to two timing filter amplifiers (TFA, Ortec 454). The outputs of the TFAs were connected to two constant fraction discriminators (CFD, Ortec 463). One of the output signals of the CFDs was directly sent to start input of the TAC, the other output was connected to stop input of the TAC through the D. The output of the TAC was sent to input of the MCA. Consequently, the time spectra of the used radioactive sources were obtained.

The output signal shapes of the TFA, CFD and TAC are shown in Figs. 12 and 13.

The rise time (the interval between the times at which the pulse reaches 10 and 90 % of its final amplitude [4]),

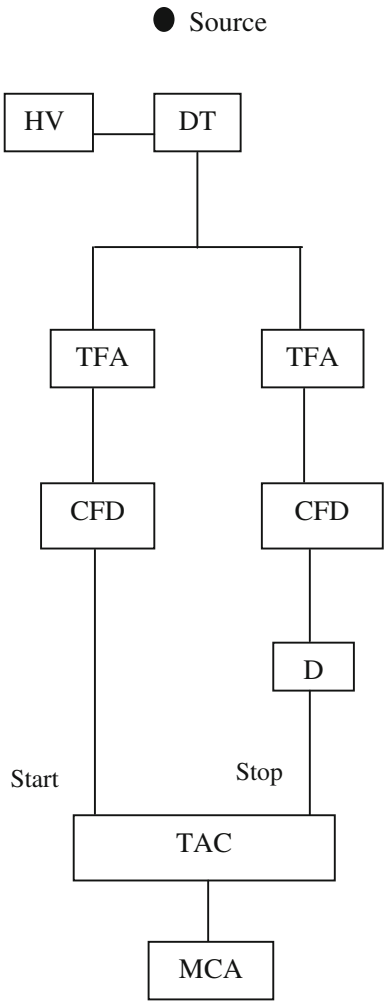


Fig. 11 *Block diagram* of the constant fraction timing method circuit (*YV* high voltage supplier, *DT* detector, *TFA* timing filter amplifier, *CFD* constant fraction discriminator, *D* delay, *TAC* time to amplitude converter, *MCA* multichannel analyzer)

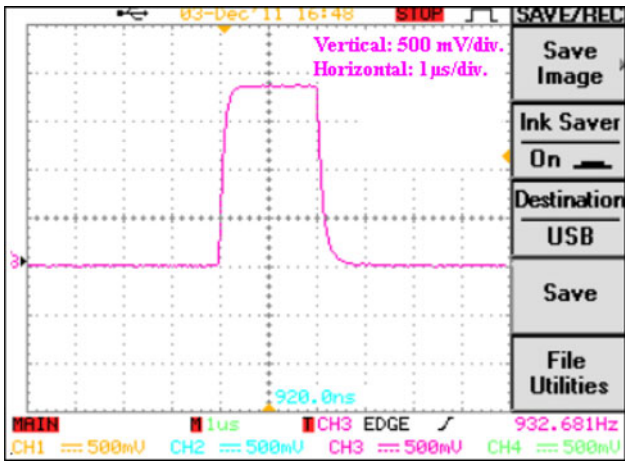


Fig. 13 Output signal shape of TAC

Table 5 Obtained parameters in constant fraction timing method (3 mm × 3 inch detector)

Source	Rise time (ns)	Fall time (ns)	Amplifier output (mV)	Constant fraction (f)	Effective constant fraction (f_{eff})
^{90}Sr	120.80	237.70	109.0	0.917	0.182
^{137}Cs	71.00	250.60	288.0	0.347	0.014
^{207}Bi	69.04	255.00	388.0	0.257	0.010

fall time (the time it takes for the signal to fall from 90 to 10 % of its full amplitude [2]), constant fraction and effective constant fraction values are given in the following tables for the used detectors. The value of the effective constant fraction was calculated by using Eq. (1) (Tables 5, 6, 7). Internal delay times (t_d) of both constant fraction discriminators were informed as 2 ns by the manufacturer [18].

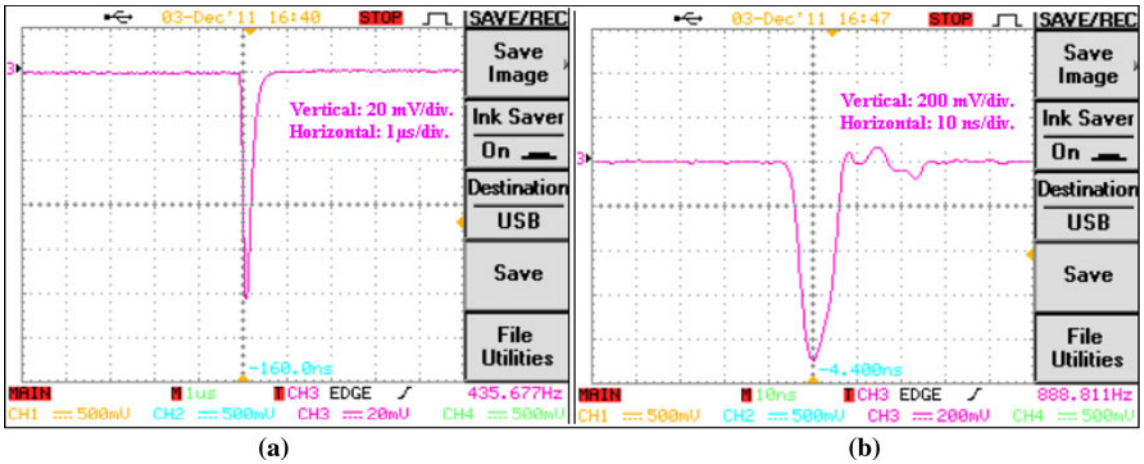


Fig. 12 Output signal shapes of **a** TFA, **b** CFD

Table 6 Obtained parameters in constant fraction timing method (0.3 mm × 3 inch detector)

Source	Rise time (ns)	Fall time (ns)	Amplifier output (mV)	Constant fraction (f)	Effective constant fraction (f_{eff})
^{90}Sr	86.41	241.80	304.0	0.328	0.011
^{137}Cs	91.41	251.60	130.0	0.769	0.072
^{207}Bi	78.14	246.50	288.0	0.347	0.013

Table 7 Obtained parameters in constant fraction timing method (9 mm × 3 inch detector)

Source	Rise time (ns)	Fall time (ns)	Amplifier output (mV)	Constant fraction (f)	Effective constant fraction (f_{eff})
^{90}Sr	72.57	249.30	672.0	0.148	0.004
^{137}Cs	67.43	238.20	248.0	0.403	0.020
^{207}Bi	72.32	259.20	544.0	0.183	0.006

Table 8 Calculated $t_r(1-f)$ values for the 3 mm × 3 inch detector

Source	$t_r(1-f)$
^{90}Sr	10.388
^{137}Cs	46.363
^{207}Bi	51.296

Table 9 Calculated $t_r(1-f)$ values for the 0.3 mm × 3 inch detector

Source	$t_r(1-f)$
^{90}Sr	58.067
^{137}Cs	21.115
^{207}Bi	51.025

Table 10 Calculated $t_r(1-f)$ values for the 9 mm × 3 inch detector

Source	$t_r(1-f)$
^{90}Sr	61.829
^{137}Cs	40.255
^{207}Bi	59.085

As stated in the previous paragraph, internal delay time ($t_d = 2$ ns) is lower than $t_r(1-f)$ value for the used detectors. This information was supported by the obtained results in Tables 8, 9, and 10.

The shaping and peaking times were found for each detector by using the information given in the previous section. The results are shown in Tables 11, 12, and 13.

When examined the results in Tables 11, 12, and 13, it is seen that the peaking times are about five times greater than the shaping times for each radioisotope. These results are in accordance with the rule depicted in the Ref. [5].

Table 11 Shaping and peaking times for the 3 mm × 3 inch detector

Source	Shaping time (ns)	Peaking time (ns)
^{90}Sr	80	440
^{137}Cs	80	400
^{207}Bi	80	400

Table 12 Shaping and peaking times for the 0.3 mm × 3 inch detector

Source	Shaping time (ns)	Peaking time (ns)
^{90}Sr	80	400
^{137}Cs	80	480
^{207}Bi	80	400

Table 13 Shaping and peaking times for the 9 mm × 3 inch detector

Source	Shaping time (ns)	Peaking time (ns)
^{90}Sr	80	360
^{137}Cs	80	400
^{207}Bi	80	400

Table 14 Time jitter and noise voltage values for the 3 mm × 3 inch detector in constant fraction timing method

Source	Time jitter (ps) (σ_T)	Noise voltage (mV) (σ_V)
^{90}Sr	120	≈12
^{137}Cs	120	≈14
^{207}Bi	120	≈16

Table 15 Time jitter and noise voltage values for the 0.3 mm × 3 inch detector in constant fraction timing method

Source	Time jitter (ps) (σ_T)	Noise voltage (mV) (σ_V)
^{90}Sr	120	≈16
^{137}Cs	120	≈16
^{207}Bi	120	≈14

It was informed that the walk time was lower than ±150 ps in the constant fraction discriminators [18].

Time jitter and noise voltage values in constant fraction timing method are given in Tables 14, 15, and 16 for each detector.

In a time spectrum which is obtained by using multi-channel analyzer, the abscissa and the ordinate correspond to the time range of a timing device and number of counts,

Table 16 Time jitter and noise voltage values for the 9 mm × 3 inch detector in constant fraction timing method

Source	Time jitter (ps) (σ_T)	Noise voltage (mV) (σ_V)
^{90}Sr	120	≈14
^{137}Cs	120	≈14
^{207}Bi	120	≈16

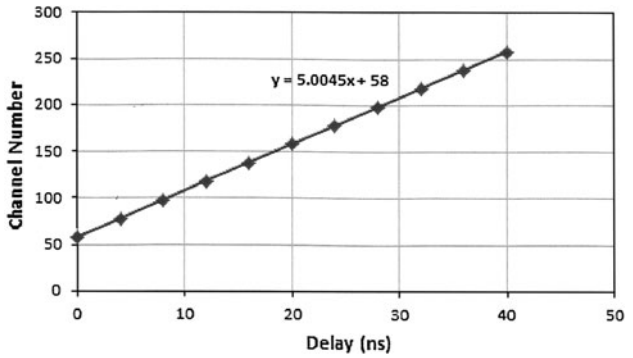


Fig. 14 Time calibration graph (fitted time calibration = 195.3125 ± 0.0051 ps/ch)

respectively. Before acquiring the time resolution results, we calibrated the channels of the MCA (time calibration). The time calibration graph is shown in Fig. 14. The inverse of the slope of this graph gives the time value per channel of the MCA. This value was calculated as 195.3125 ± 0.0051 ps. Time per channel was also obtained as 195 ps from the MCA. These values are in accordance with each other, signifying good time calibration was acquired.

Results

Leading edge timing method

In leading edge timing method, the time spectra of ^{90}Sr, ^{137}Cs and ^{207}Bi radioisotopes for each detector are shown in Figs. 15, 16, 17, 18, 19, 20, 21, 22, and 23.

Constant fraction timing method

In constant fraction method, the obtained time spectra of ^{90}Sr, ^{137}Cs and ^{207}Bi radioisotopes for each detector can be seen in Figs. 24, 25, 26, 27, 28, 29, 30, 31, and 32.

Horizontal and vertical axes correspond to channel and counts, respectively in these figures above.

It can be concluded that the obtained time spectra have no pile-up and spectrum distortion effects because the dead time of the MCA is lower than 30–40 % level [2, 4].

Time resolution values from leading edge and constant fraction timing methods are shown in Tables 17, 18, and 19 for each detector.

Discussion

Timing methods determine the point of the time development of the pulse, but each timing method chooses this point in different way [12]. Therefore, leading edge and constant fraction timing methods were used in this study.

Effective constant fraction value was calculated through Eq. (1). As stated in the previous section, we found that the effective constant fraction value was lower than the constant fraction value for each detector. This result is in accordance with the literature [16].

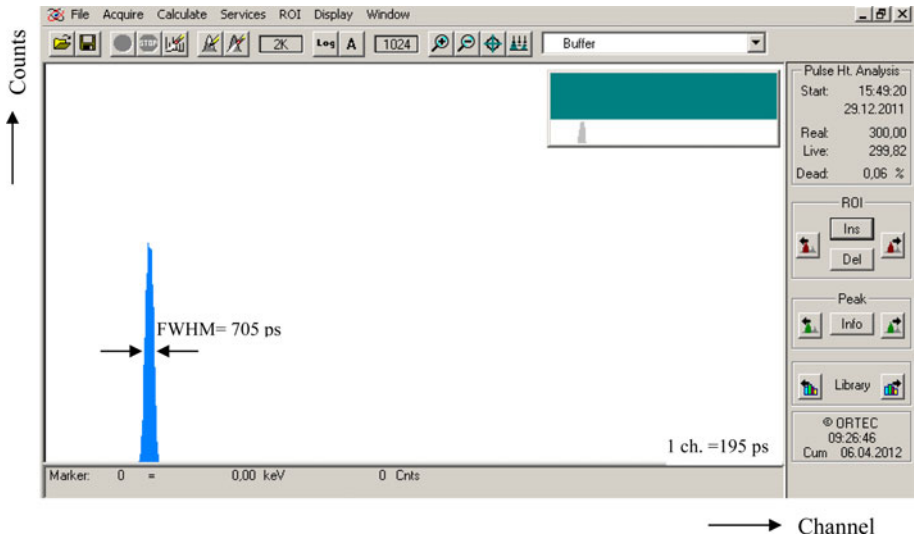


Fig. 15 Time spectrum of ^{90}Sr from 3 mm × 3 inch plastic scintillation detector

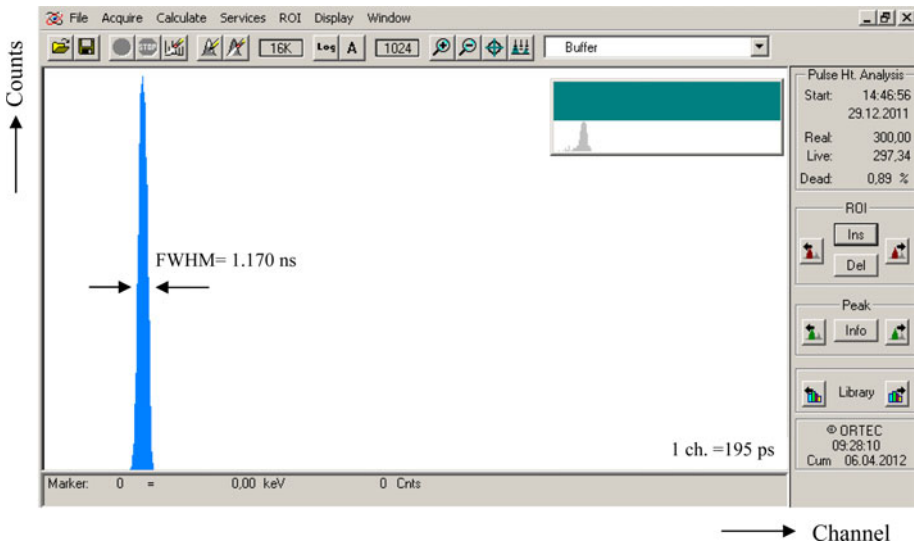


Fig. 16 Time spectrum of ^{137}Cs from 3 mm × 3 inch plastic scintillation detector

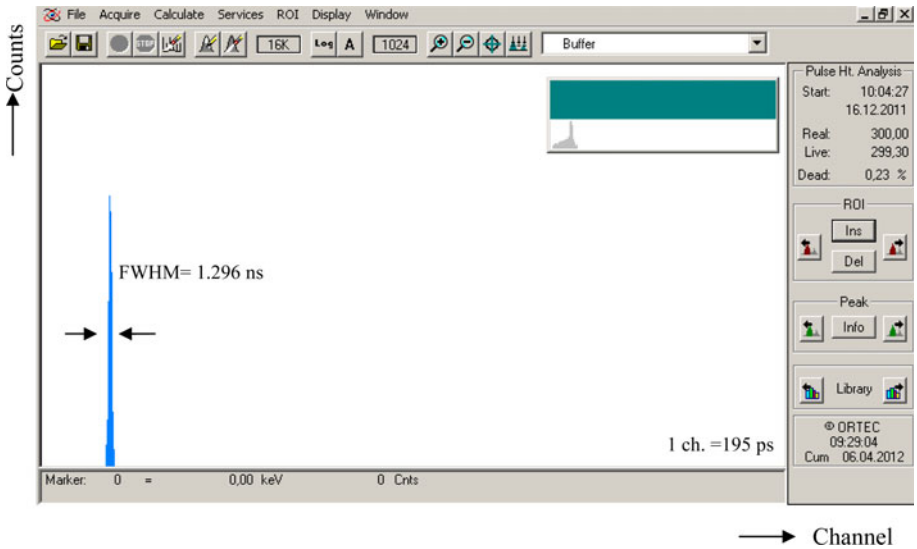


Fig. 17 Time spectrum of ^{207}Bi from 3 mm × 3 inch plastic scintillation detector

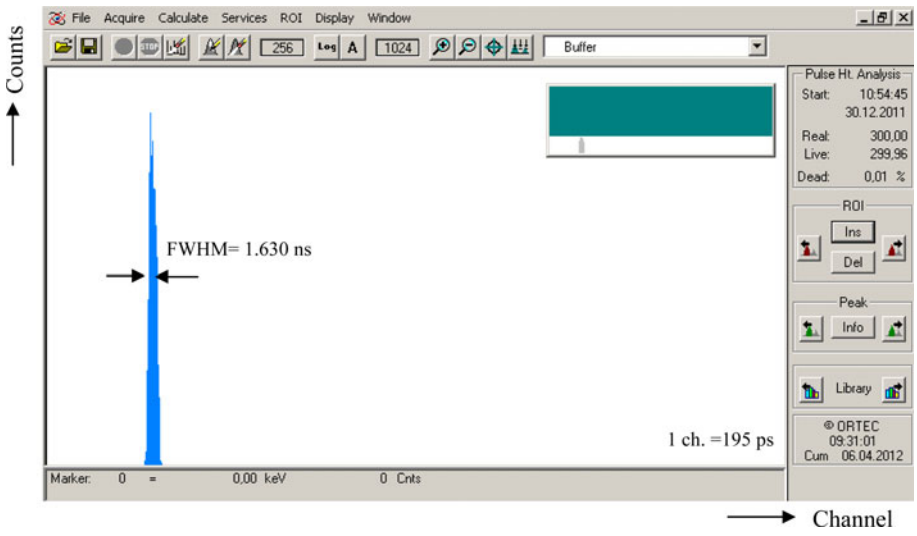


Fig. 18 Time spectrum of ^{90}Sr from 0.3 mm × 3 inch plastic scintillation detector

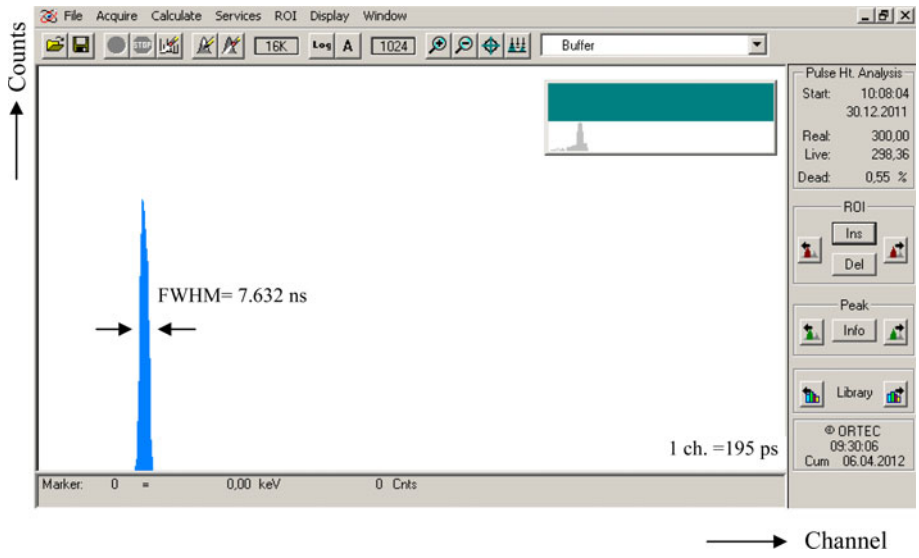


Fig. 19 Time spectrum of ^{137}Cs from 0.3 mm × 3 inch plastic scintillation detector

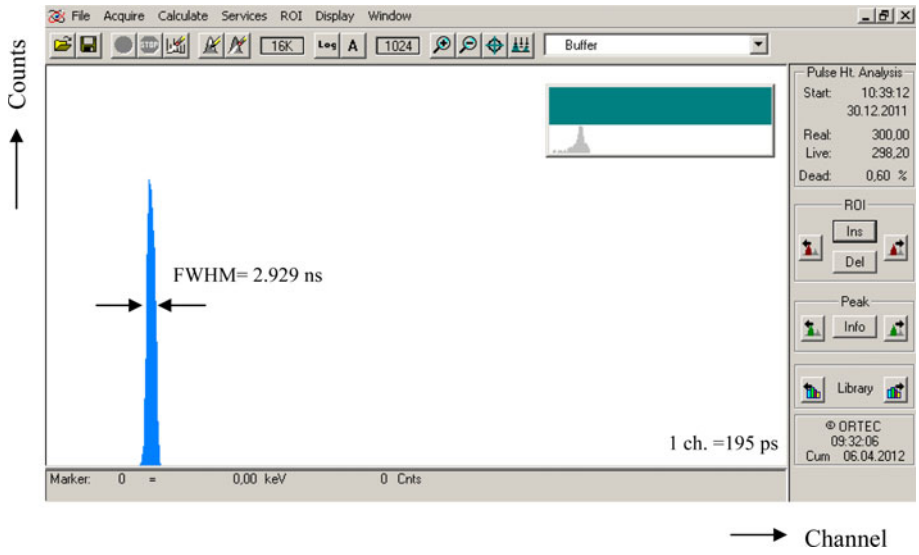


Fig. 20 Time spectrum of ^{207}Bi from 0.3 mm × 3 inch plastic scintillation detector

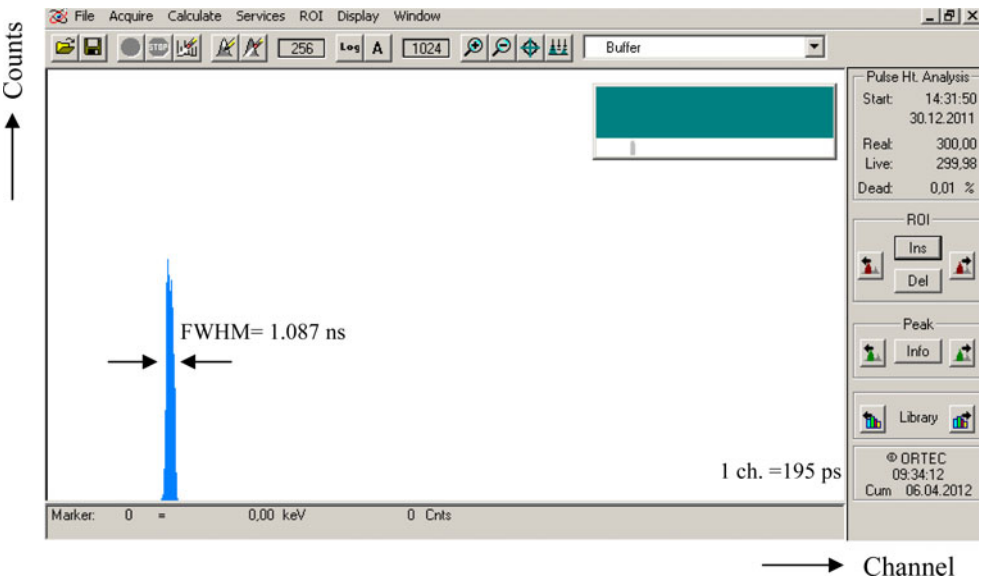


Fig. 21 Time spectrum of ^{90}Sr from 9 mm × 3 inch plastic scintillation detector

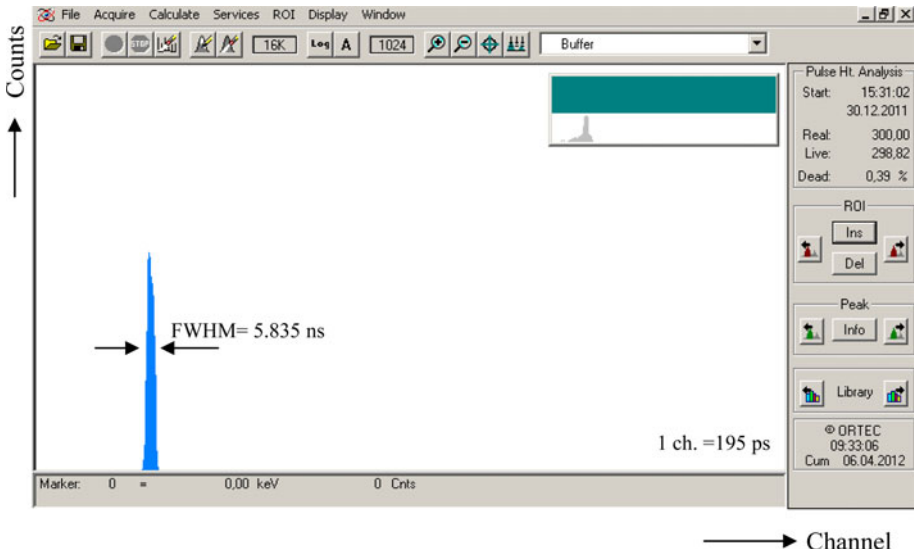


Fig. 22 Time spectrum of ^{137}Cs from 9 mm × 3 inch plastic scintillation detector

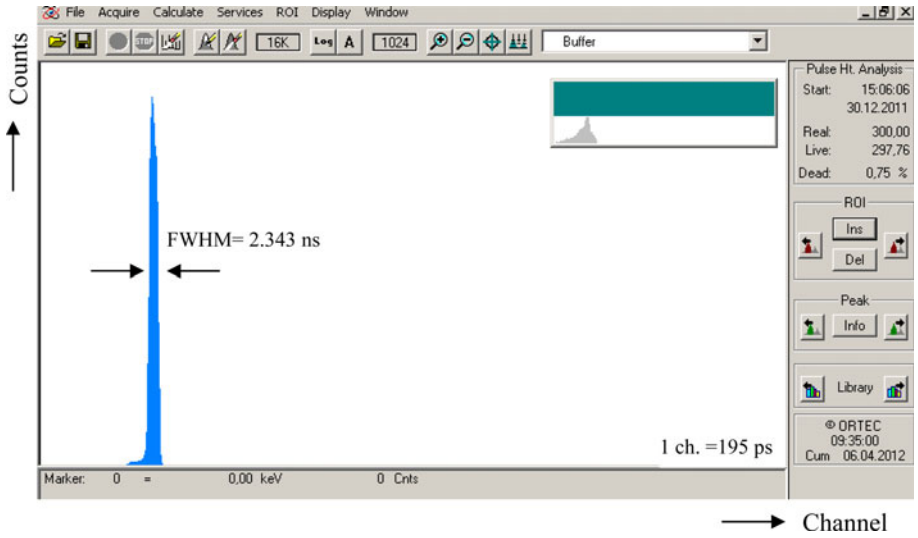


Fig. 23 Time spectrum of ^{207}Bi from 9 mm × 3 inch plastic scintillation detector

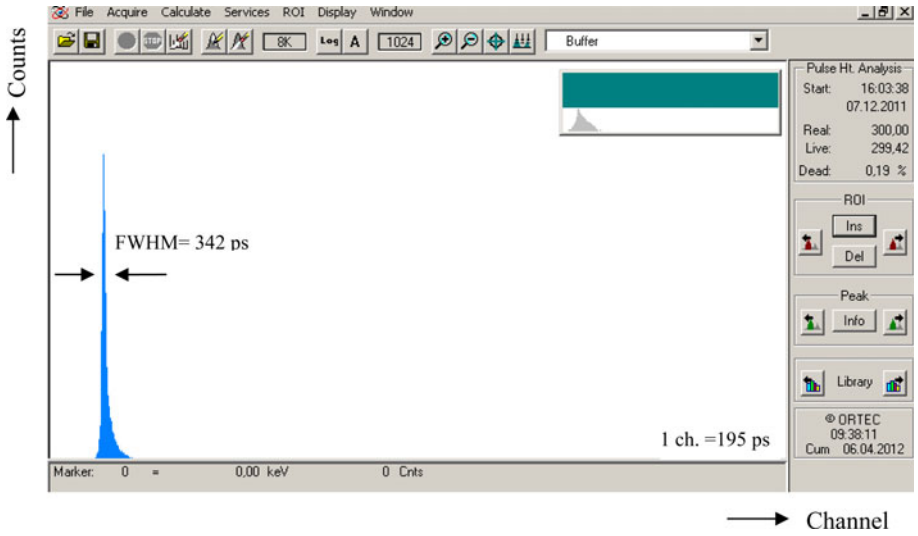


Fig. 24 Time spectrum of ^{90}Sr from 3 mm × 3 inch plastic scintillation detector

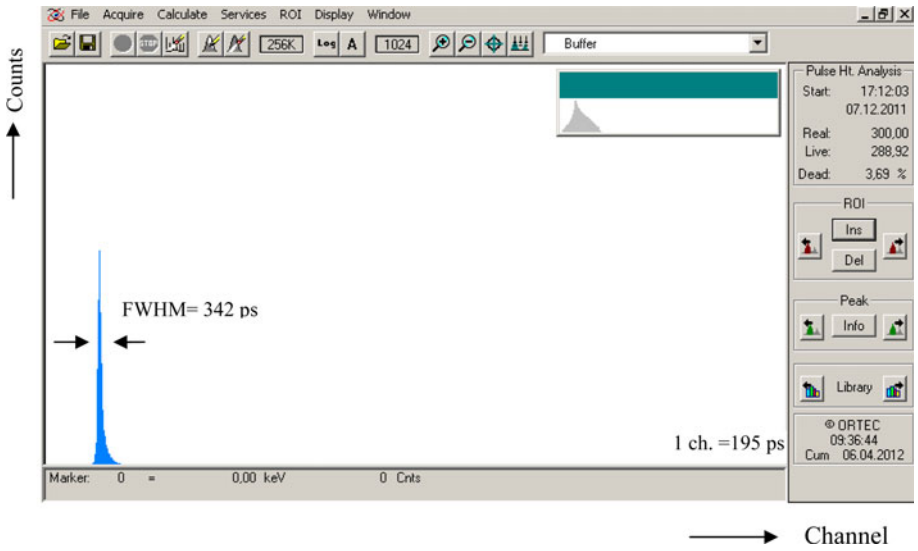


Fig. 25 Time spectrum of ^{137}Cs from 3 mm × 3 inch plastic scintillation detector

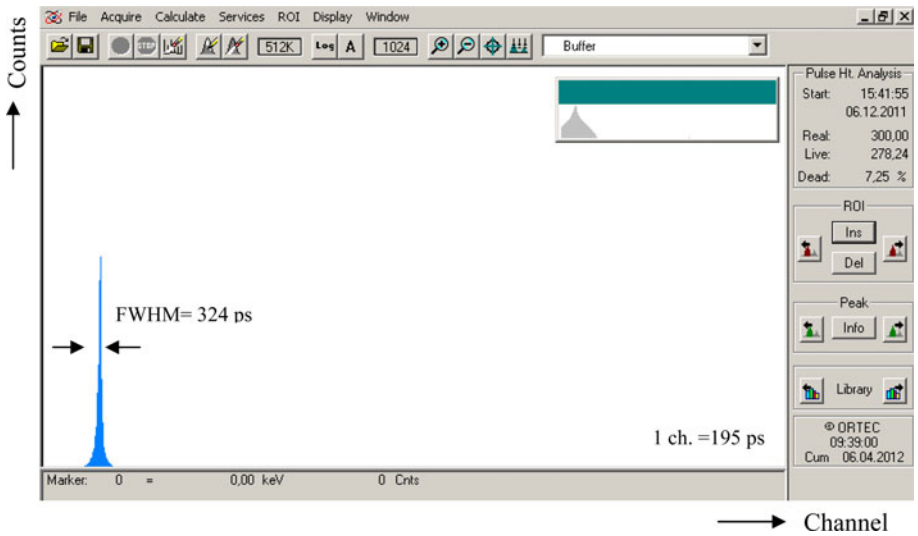


Fig. 26 Time spectrum of ^{207}Bi from 3 mm × 3 inch plastic scintillation detector

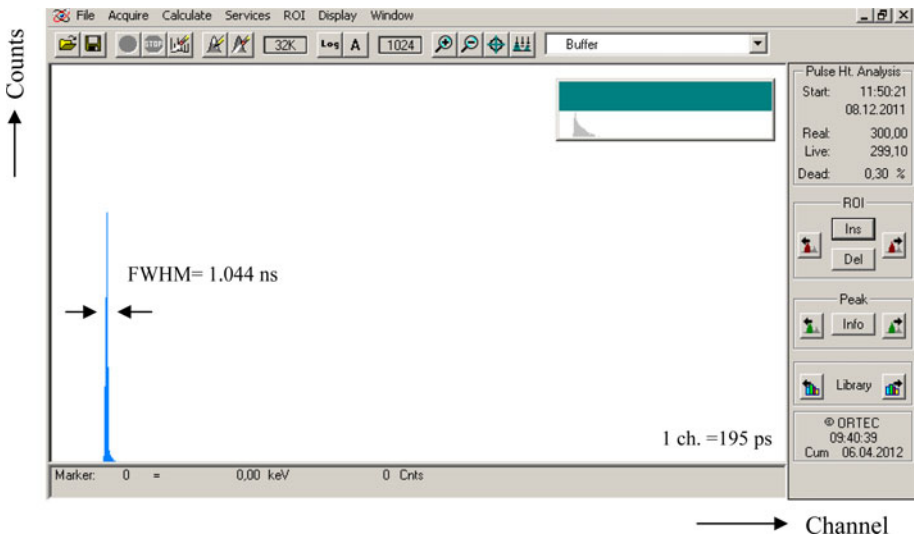


Fig. 27 Time spectrum of ^{90}Sr from 0.3 mm × 3 inch plastic scintillation detector

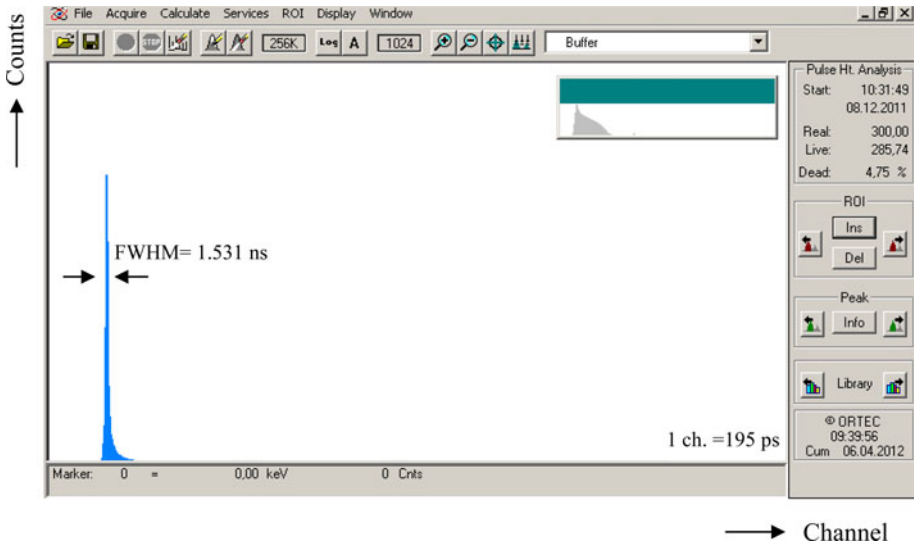


Fig. 28 Time spectrum of ^{137}Cs from 0.3 mm × 3 inch plastic scintillation detector

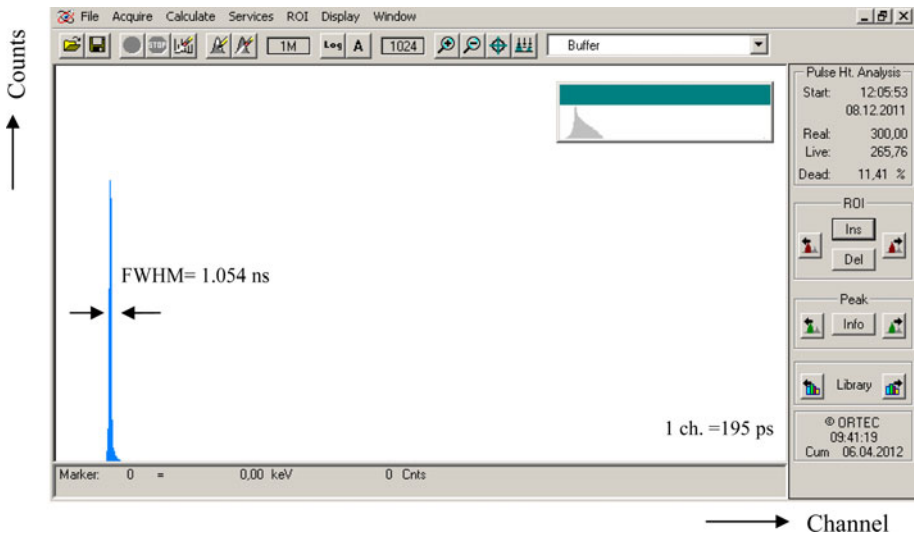


Fig. 29 Time spectrum of ^{207}Bi from 0.3 mm × 3 inch plastic scintillation detector

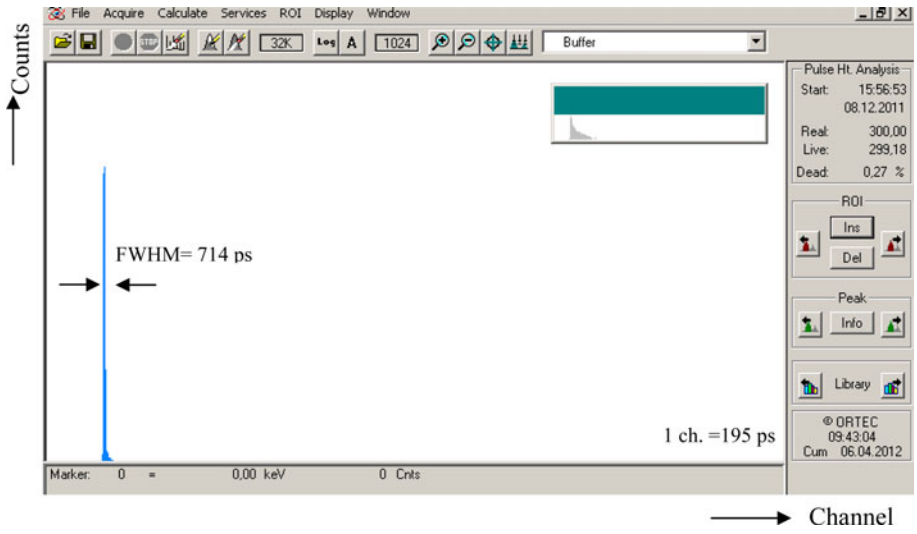


Fig. 30 Time spectrum of ^{90}Sr from 9 mm × 3 inch plastic scintillation detector

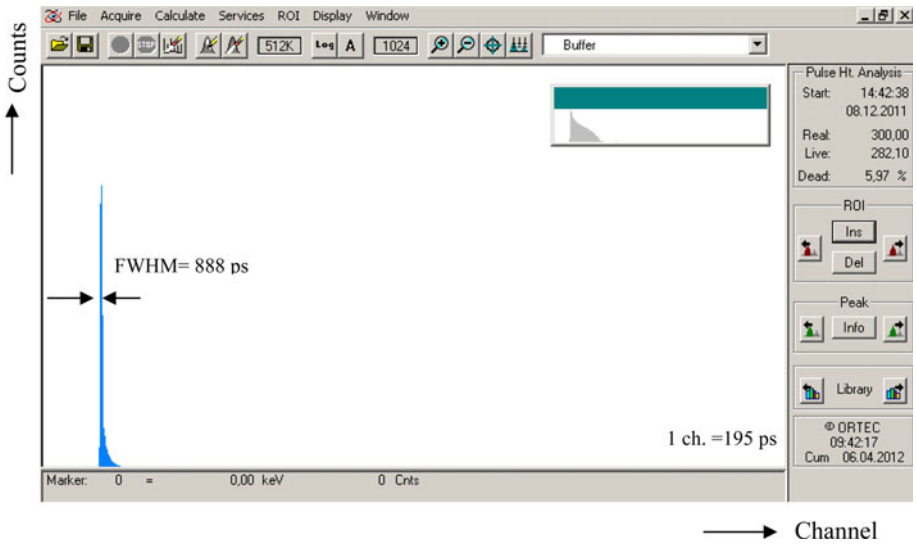


Fig. 31 Time spectrum of ^{137}Cs from 9 mm × 3 inch plastic scintillation detector

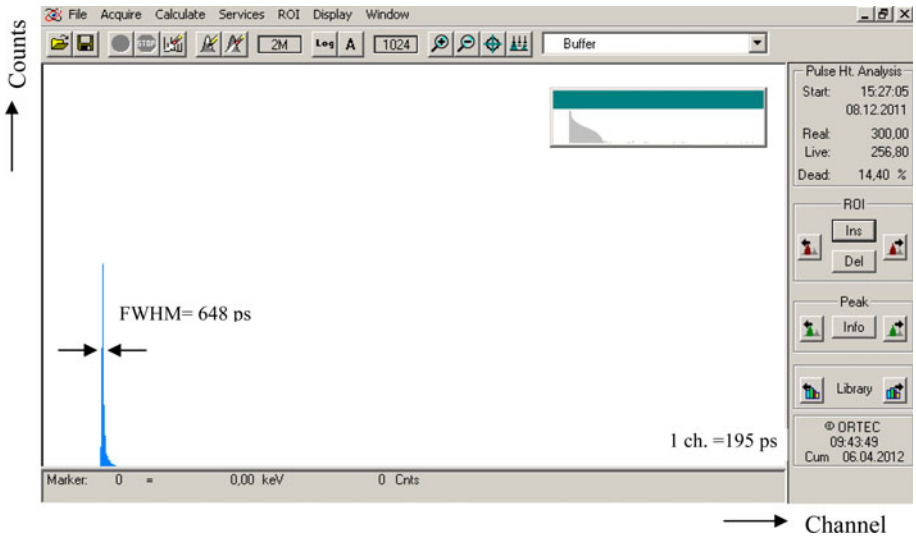


Fig. 32 Time spectrum of ^{207}Bi from 9 mm × 3 inch plastic scintillation detector

Table 17 Comparison of the time resolution values from both timing methods for 3 mm × 3 inch detector

Radioactive source	Time resolution value in leading edge timing method (ns)	Time resolution value in constant fraction timing method (ns)
^{90}Sr	0.705	0.342
^{137}Cs	1.770	0.342
^{207}Bi	1.296	0.324

Table 18 Comparison of the time resolution values from both timing methods for 0.3 mm × 3 inch detector

Radioactive source	Time resolution values in leading edge timing method (ns)	Time resolution values in constant fraction timing method (ns)
^{90}Sr	1.630	1.044
^{137}Cs	7.632	1.531
^{207}Bi	2.929	1.054

Internal delay time in constant fraction discriminator was informed as 2 ns by the manufacturer [18]. Delay times were calculated by using Eq. (2) for the used detectors (Tables 8, 9, 10). In this way, the validity of this equation was proved.

As shown in Tables 17, 18, and 19, the time resolution values obtained from constant fraction timing method are lower than those of leading edge timing method. This means that the obtained time resolution values from constant fraction timing method are better than those of leading edge timing method as informed in various studies [2, 3, 16]. Since walk effect is more explicit in leading edge timing method than constant fraction timing method due to the signal amplitude change, constant fraction timing method provided better time resolution values [3].

Table 19 Comparison of the time resolution values from both timing methods for 9 mm × 3 inch detector

Radioactive source	Time resolution values in leading edge timing method (ns)	Time resolution values in constant fraction timing method (ns)
^{90}Sr	1.087	0.714
^{137}Cs	5.835	0.888
^{207}Bi	2.343	0.648

In addition, better time resolution results were obtained depending on the optimum detector thickness for the monoenergetic particle energy.

Consequently, this work may be an auxiliary reference source for the researchers who work in timing measurements with general purpose plastic scintillation detectors.

Acknowledgments This work was supported by TUBITAK, the Scientific and Technical Research Council of TURKEY under Projects No. 111T571 and 197T087, and by EBILTEM, Center of Science and Technology, Ege University under Project No. 99 BIL 001.

References

1. Martoiu S, Rivetti A (2011) Electronics for radiation detection. CRC Press, USA
2. Leo RW (1987) Techniques for nuclear and particle physics experiments. Springer, Berlin
3. Moszynski M, Bengston B (1979) Nucl Instrum Meth 151:1–31
4. Knoll GF (2000) Radiation detection and measurements. Wiley, New York
5. Bönisch SP (2011) Electronics for radiation detection. CRC Press, USA
6. Ortec AN42 Application Note-Principles and Applications of Timing Spectroscopy
7. http://www.detectors.saint-gobain.com/Plastic-Scintillator.aspx Accessed 11 April 2012
8. Abuelhia E, Alzimami K, Alkhorayef M, Podolyak Z, Spyrou NM (2008) J Radioanal Nucl Chem 278:767–771
9. Puzovic JM, Anicin IV (2007) Nucl Instrum Meth A 572: 926–928
10. Zaitseva N, Rupert BL, Pawelczak I, Glenn A, Martinez HP, Carman L, Faust M, Cherepy N, Payne S (2012) Nucl Instrum Meth A 668:88–93
11. http://www.matpack.de/Info/Nuclear/Nuclids/nuclids9.html Accessed 11 April 2012
12. Tsoulfanidis N (1995) Measurements and detection of radiation. Taylor & Francis, USA
13. Model 460 Delay Line Amplifier Catalogue
14. Nutt R, Gedcke DA, Williams CW (1970) IEEE Trans Nucl Sci 17:299–306
15. Gedcke DA, McDonald WJ (1968) Nucl Instrum Meth 58: 253–260
16. Paulus TJ (1985) IEEE Trans Nucl Sci 32:1242–1249
17. Jackson RG, Blalock TV (1997) IEEE Trans Nucl Sci 44:303–307
18. Model 463 Constant Fraction Discriminator Catalogue